https://doi.org/10.1016/j.actbio.2024.01.024

Cell mechanics regulate the migration and invasion of hepatocellular carcinoma cells via JNK signaling

Junfan Wang[1,2], Bai Zhang[1,2], Xi Chen[1,2], Ying Xin[1,2], Keming Li[1,2], Cunyu Zhang[1,2], Kai Tang[1,2] and Youhua Tan [1,2,*]

[1]The Hong Kong Polytechnic University Shenzhen Research Institute, Shenzhen 518000, China

[2]Department of Biomedical Engineering, The Hong Kong Polytechnic University, Hong Kong 999077, China

*Correspondence: youhua.tan@polyu.edu.hk

Keywords: cell mechanics, actomyosin, motility, metastasis, hepatocellular carcinoma

Abstract

Hepatocellular carcinoma (HCC) cells, especially those with metastatic competence, show reduced stiffness compared to the non-malignant counterparts. However, it is still unclear whether and how the mechanics of HCC cells influence their migration and invasion. This study reports that HCC cells with enhanced motility show reduced mechanical stiffness and cytoskeleton, suggesting the inverse correlation between cellular stiffness and motility. Through pharmacologic and genetic approaches, inhibiting actomyosin activity reduces HCC cellular stiffness but promotes their migration and invasion, while activating it increases cell stiffness but impairs cell motility. Actomyosin regulates cell motility through the influence on cellular stiffness. Mechanistically, weakening/strengthening cells inhibits/promotes c-Jun N terminal kinase (JNK) phosphorylation, activation/inhibition of which rescues the effects of cell mechanics on their migration and invasion. Further, HCC cancer stem cells (CSCs) exhibit higher motility but lower stiffness than control cells. Increasing CSC stiffness weakens migration and invasion through the activation of JNK signaling. In conclusion, our findings unveil a new regulatory role of actomyosin-mediated cellular mechanics in tumor cell motility and present new evidence to support that tumor cell softening may be one driving force for HCC metastasis.

Introduction

Metastasis is the leading threat to cancer patients, as it is responsible for over 90% of cancer-related deaths [1, 2]. Hepatocellular carcinoma (HCC) ranks as one of the deadliest cancer types because of high chemoresistance, recurrence rate and frequent metastasis [3]. Many biochemical factors have been reported to play critical roles in metastasis [4, 5], which has advanced the development of various therapeutic strategies by targeting different pro-metastatic signaling [6, 7]. However, there is increasing

unmet demand in improving the outcomes of clinical HCC patients with metastasis, which necessitates the comprehensive understanding of the mechanisms underlying tumor metastasis from a broad perspective.

Despite the classical view that genetic mutation drives cancer initiation and progression, the roles of mechanical cues in tumor metastasis have been increasingly appreciated [8, 9]. In particular, oncogenic mutation-induced transformation is accompanied with the alterations of cellular stiffness during tumor initiation [10, 11]. Accumulating evidence shows that cancer cells are much softer than their healthy counterparts in various types of cancer, including breast, colon, ovarian, bladder, and liver cancer [12-16]. For example, the mechanical stiffness of breast cancer cells is strongly correlated with their malignancy [17]. Recent evidence shows that the soft cells isolated from a whole tumor cell population exhibit high stemness and tumorigenic potential [16]. Low cellular stiffness is associated with high invasiveness and stemness [18-21]. Metastatic tumor cells display higher deformability and compliance than their counterparts with low metastatic capacity both in cancer cell lines and patient-derived primary tumor cells [22, 23]. Cancer stem cells (CSCs) are believed to be the seeds of cancer metastases and show lower stiffness than non-CSCs [24]. During the metastatic process, tumor cells encounter different microenvironmental cues [8] so that disseminated tumor cells may need to alter their cellular mechanical properties to adapt to distinct mechanical microenvironments at every metastatic stage [25]. For example, low stiffness facilitates the trans-endothelial migration of tumorigenic cells and thus promotes the extravasation of circulating tumor cells [17]. Disseminated tumor cells that survive under blood shear stress show reduced cellular stiffness, and low stiffness enhances the survival of these cells under fluid shear stress [26]. However, it is still unclear whether tumor cell softening is the cause or consequence of tumor metastasis.

In this study, the relationship between the stiffness of HCC cells and their migration

and invasion was explored. To examine the roles of tumor cell mechanics, cellular stiffness was modulated by pharmacologically and genetically targeting cytoskeleton, RhoA, Rho-associated protein kinase (ROCK), myosin light chain kinase (MLCK), and myosin II. The influence of the mechanical alteration on the motility of HCC cells was evaluated. A mechanistic study was further conducted to explore the underlying mechanism by which cellular stiffness regulates HCC migration and invasion, especially c-Jun N-terminal kinase (JNK) signaling.

Materials and Methods

Cell culture

Human HCC cell lines HepG2, MHCC97-L, and Huh-7 were kindly provided by Prof. Terence Lee from Hong Kong Polytechnic University. Cells were maintained with Dulbecco's Modified Eagle Medium (DMEM; HyClone Laboratories, Logan, UT) supplemented with 10% fetal bovine serum (HyClone Laboratories) and 1% penicillin/streptomycin (HyClone Laboratories) in cell culture flask or petri dishes at 37°C and 5% CO_2. Cells were passaged every 3-4 days using 0.25% trypsin (HyClone Laboratories).

Cell culture in 3D fibrin

Salmon fibrinogen and thrombin were purchased from Searun Holdings (San Diego, CA, USA). Fibrinogen was diluted into 2 mg/mL with T7 buffer (pH 7.4, 50 mM Tris, 150 mM NaCl). HCC cells were detached and suspended in DMEM with 10% FBS and 1% penicillin/streptomycin. Cell suspension and fibrinogen solution were mixed equally to prepare 1 mg/mL fibrinogen. 6 μL thrombin (0.1 U/μL) was pre-added to each well of 24 well-plate at the bottom, and 300 μL cell-fibrinogen solution was then seeded into each well. After the gentle mixing of fibrinogen and thrombin solution, the plate was moved into 37°C cell culture incubator for 15 min. Finally, 1 mL full culture

medium was gently added into each well. The 24 well-plate was transferred to 37°C incubator supplemented with 5% CO_2.

Pharmacologic treatment

All inhibitors and activators were dissolved in DMSO to prepare the stock solution according to the manufacturer's instructions. The stock solution was diluted into the working concentration by full culture medium. DMSO was used as the control group. For pre-treatment, HCC cells were seeded in 6-well plates with around 70%-80% confluency. Cells were then treated with 10 μM Y-27632 (Selleck Chemicals, Houston, TX), 10 μM Blebbistatin (Sigma-Aldrich, St. Louis, MO, USA), 0.5 μM Cytochalasin D (Tocris Bioscience, Bristol, United Kingdom), 10 nM or 0.1 μM Jasplakinolide (Selleck Chemicals, Houston, TX, USA), 5 nM or 20 nM Narciclasine (Selleck Chemicals, Houston, TX, USA), 50 nM Anisomycin (Selleck Chemicals, Houston, TX, USA) and 20 nM SP600125 (Selleck Chemicals, Houston, TX, USA) for the indicated durations. In 3D tumor spheroid invasion assay, 20 μM Y-27632, 20 μM Blebbistatin, 0.1 μM Jasplakinolide, or 20 nM Narciclasine were added on the top of 3D collagen gels.

Cell transfection

Lipofectamine 3000 reagent (Thermo Fisher Scientific, Waltham, MA) was used for siRNA and plasmid transfection. siRNAs were designed and synthesized by Hanbio Biotechnology Co., Ltd. (Shanghai). The specific siRNA sequence for MLCK, mDia1, and control is 5′-GGACGAUUCUCCUGCAAGA-3′, 5′-GUGUGUCUCUCAACAACAA-3′, and 5′-UUCUCCGAACGUGUCACGU-3′, respectively. pSLIK empty vectors, CA-ROCK, and CA-MLCK plasmids were kind gifts from Prof. Sanjay Kumar in University of California, Berkeley. Cells were seeded into a 6-well cell culture plate until the confluence reached around 60%-70%. Lipofectamine 3000 reagent and siRNAs or plasmids were diluted by Opti-MEM. For

diluted plasmids, P3000 reagent was added. Diluted Lipofectamine 3000 and siRNAs or plasmids were mixed together with the same amount and incubated at room temperature for 15 min. The mixture was then added to the cells for 2 days. 50 ng/mL doxycycline (TargetMol, Wellesley, MA) was added to the cells transfected with the CA plasmids for another 2 days. The transfection efficiency was validated by quantitative RT-PCR analysis and western blotting.

Measurement of cellular stiffness by atomic force microscope (AFM)

Cell stiffness was measured using a Bruker Catalyst AFM (Bruker, Billerica, MA, USA) coupled with an inverted microscope (Nikon, Tokyo, Japan). Silicon nitride cantilevers (MLCT, Bruker, Billerica, MA, USA) with a nominal spring constant of 0.02 N/m were adopted for measurement. The probe sensitivity and spring constant were calibrated in culture medium. Cells were plated on collagen-coated glass slides for 12 h and spread well before the experiments. To determine the cellular locations for stiffness measurement, the nucleus of a cell was located under the bright field of an inverted microscope. The middle point between the centre of the nucleus and the cell boundary was chosen as the indentation area. When the biological sample is indented by more than 10-15% of the thickness, the effect from the underlying substrate needs to be considered [27]. Cells are normally viscoelastic and can be assumed to be linearly elastic when the strain is small (<10-15%) and the loading rate is low (1 μm/s) [28]. In this study, the thickness of the probed cell area was ~5-6 μm (Supplementary Figure 1j). It was reasonable to neglect the substrate effect when the indentation depth was 500 nm and assume the linear elasticity of cell material in this direction with controllable error. Five force-indentation curves were recorded from the corresponding sites around the indentation area for each cell. The Young's modulus was analyzed and determined with Nanoscope Analysis 1.9 Software (Bruker, Karlsruhe, Germany) through fitting with Sneddon's modification of the Hertzian model. To minimize the potential

influence, cells were kept at room temperature within 1 h for stiffness measurement. No obvious changes in cell morphology during the course of AFM measurement were observed.

Wound healing assay

Cells were seeded into 24-well plates until reaching 90%-100% confluency. 200 μL tips were used to make a uniform scratch on the cell monolayer. The cells were washed three times by phosphate buffer solution (PBS) and incubated at 37°C supplemented with 5% CO_2. Photos of scratch were taken at 0, 24, and 48 h. The percentage of the scratch closure was calculated as the ratio of the migrated area at the time point of 0, 24 and 48 h over the wound area at 0 h using ImageJ (National Institutes of Health, Bethesda, MD, USA).

Transwell migration and invasion assay

In vitro migration assay was conducted using Transwell cell culture chambers (8 μm pore polycarbonate, Corning Costar, USA). HCC cells (1×10^5) were placed into the upper chamber with DMEM while the bottom well was filled with 600 μL full cell culture medium. After being incubated at 37 °C, 5% CO2 for 24 h, the top surface of the chamber was cleaned by cotton swab and the bottom surface was stained with 0.1% crystal violet for 15-20 min. The number of migrated cells was counted in five representative fields per insert. For Transwell invasion assay, the upper chamber was coated with 80μl Corning® Matrigel® basement membrane matrix (diluted by DMEM to the concentration of 2 mg/mL in advance) before seeding cells. Cells were placed on top of the Matrigel at 2×10^5/chamber in serum-free DMEM medium for 48 h. Cotton swabs were utilized to gently scrap the top of the Transwell membrane and carefully remove the remaining tumor cells. The invaded cells within the gel were stained and quantified.

3D tumor spheroid invasion assay in collagen gels

HCC cells were trypsinized to single cells, counted, and resuspended in DMEM at the concentration of $1x10^5$ cells/mL. Every 20 μL of the cell solution was dropped on the top of a coverslip, which was then overturned. Drops were left without shaking for 48 h in the incubator until tumor spheroids were formed. Neutralized collagen I solution was prepared at a final concentration of 1.0 mg/mL, containing 10% 10X DMEM, 1% human insulin solution (Sigma-Aldrich, St. Louis, MO, USA), and sterilized PBS. The pH was adjusted to 7.4 by gradually adding 0.1M NaOH. The 96-well cell culture plate was coated with 50 μL neutralized collagen I solution and then transferred to an incubator at 37°C for at least 30 min until the collagen was polymerized. Tumor spheroids were mixed with neutralized collagen I solution and added into the pre-coated 96-well plate, which was then incubated at 37°C and 5% CO_2 until collagen was polymerized. 50 μL pre-warmed culture medium or working solution containing the corresponding inhibitors/activators was slowly and gently added on the top of collagen gels. The invasion was monitored under 10X objective lens during the next two days and the images were captured at 0, 24 and 48h after embedding. The area covered by spheroids at each time point was measured by ImageJ software (National Institutes of Health, Bethesda, MD). The change of spheroid area was calculated and normalized to the area at 0 h. Invasion index represented the relative value of spheroid area change.

MTS assay

The 3-(4,5-dimethylthiazol-2-yl)-5-(3-carboxymethoxyphenyl)-2-(4-sulfophenyl)-2H-tetrazolium (MTS) assay was performed to measure cell viability according to the manufacturer's instructions (Promega, Madison, WI, USA). 100 μL of cell suspension was collected after treatment and then added to a well of the 96-well plate. After incubation for 12 h until all cells adhered to the bottom of the well, 20 μL of sterile CellTiter 96 aqueous solution (5 mg/mL; Promega, Madison, WI, USA) was added to each well in dark, and the plate was incubated for 4 h at 37 °C without light. The

absorbance of the cell solution was measured at 490 nm using a Benchmark Plus microplate reader (Bio-Rad, Hercules, CA, USA).

Quantitative RT-PCR analysis

E.Z.N.A.® Total RNA Kit (Omega, Norcross, GA, USA) was used to extract total RNA from cells and the complementary DNAs were synthesized by the RevertAid First Strand cDNA Synthesis Kit (Thermo, Waltham, MA, USA). Quantitative RT-PCR was performed using Forget-Me-Not EvaGreen qPCR Master Mix with Rox (Biotium, San Francisco, CA, USA) and CFX96 Real-Time System (Bio-Rad, Hercules, CA, USA). The primer sequences were listed in supplementary Table 1. Relative gene expression was evaluated by using the ΔΔCT method and normalized to the expression of human glyceraldehyde 3-phosphate dehydrogenase (GAPDH).

F-actin staining

CytoPainter F-actin labeling kit (Abcam, Cambridge, MA, USA) was used to stain F-actin. The cells were first fixed with 4% paraformaldehyde for 15 min at room temperature and permeabilized by 0.1% Triton X-100 in PBS for 5-10 min. Then, the cells were stained with 1× green fluorescence Phalloidin conjugate working solution at room temperature for 1 h. The treated cells were washed gently for 3 times by PBS and stained with DAPI before imaging by the inverted fluorescent microscope (Nikon) using FITC and DAPI channel, respectively. Fluorescence intensity was quantified using ImageJ software (National Institutes of Health, Bethesda, MD).

Western blotting analysis

Cells were lysed by RIPA lysis buffer and extraction buffer (Thermo Fisher, MA) with Halt Phosphatase Inhibitor Cocktail (Thermo fisher, MA), placed on the ice for 30 min and centrifuged at 13000 rpm, 4°C for 30 min. The protein concentration was determined by the BCA kit (Beijing Solarbio Science & Technology Co., Ltd). The protein was denatured at 95°C for 10 min and then run on an 10% SDS–PAGE gel and

transferred to Nitrocellulose (NC) membrane with a pore size of 0.2/0.44 μm using Trans-Blotting Turbo (Bio-Rad). The NC membrane containing proteins was blocked in 5% bovine serum albumin (BSA) and probed with corresponding primary antibody at 4°C overnight. Secondary antibodies conjugated to horseradish peroxidase were utilized for enhanced chemiluminescence (Thermo fisher, MA). Images were taken using Clarity™ and Clarity Max™ Western Enhanced Chemiluminescence Blotting Substrates and ChemiDoc™ MP Imaging System (Bio-Rad).

Immunofluorescence staining

For immunofluorescence staining, cells were seeded on the coverslips and fixed with 4% paraformaldehyde for 15 min, permeabilized in 0.2% Triton X-100 for 10 min, washed three times with PBS, and blocked with blocking buffer (PBS, 1% BSA, 0.1% Tween-20, and 0.2% Triton X-100) at room temperature for 30 min. Cells were stained with diluted primary antibody at 4°C overnight, and washed three times with PBS. The samples were incubated with diluted secondary antibodies at room temperature for 1 h and washed three times by PBS. After that, slides were counterstaining and mounted with 4′,6-diamidino-2- phenylindole (DAPI, Invitrogen). Fluorescent images were captured under a fluorescent microscope (Nikon, Tokyo, Japan) using PE, FITC, and DAPI channels, respectively. Fluorescence intensity was analyzed using ImageJ (National Institutes of Health, Bethesda, MD, USA).

Cell morphology measurement

The cells were seeded into collagen-coated 24-well plate and incubated at 37 °C supplemented with 5% CO_2 for 12 h. The cells were washed with PBS gently to remove the non-adhered cells. Images were captured using the inverted microscope (Nikon, Tokyo, Japan). Cell spreading area and aspect ratio were quantified by the ImageJ software (National Institutes of Health, Bethesda, MD).

F-actin/G-actin ratio measurement

F-actin/G-actin ratio measurement assay was performed according to the manufacturer's instructions of G-actin/F-actin In Vivo Assay Kit (Cytoskeleton, Denver, CO). In brief, cells were obtained after different pre-treatments and lysed by LAS2 buffer (containing Lysis and F-actin Stabilization Buffer, ATP solution, and protease inhibitor cocktail stock). The lysate was homogenized, incubated at 37℃ for 10 min and centrifuged at 2000 rpm for 5 min at room temperature. Then, the supernatant was transferred to an ultrafast centrifuge tube (Beckman Coulter) and centrifuged at 100,000 g for 1 h by ultracentrifuge (Beckman Coulter, Optima MAX-XP). The supernatant contained soluble G-actin and the pellet left on the bottom of the tube was F-actin. F-actin depolymerization buffer was added to the F-actin pellet on ice for 1 h and pipetted up and down every 15 min to accelerate F-actin pellet resuspension. The expression levels of F-actin and G-actin were quantified and analyzed by SDS-PAGE and western blot assay.

Statistical analysis

All the results were shown as mean ± SEM (standard error of the mean) in this study and at least three independent repeats were conducted for each experiment. Two-tailed Student's t-test was applied for the comparison between two groups, while ANOVA analysis was conducted when there were three or more conditions. The post hoc Tukey or Bonferroni test was adopted for the comparisons with equal or unequal sample sizes, respectively. n.s.: no significance, *, $p < 0.05$, **, $p < 0.01$ ***, $p < 0.001$, ****. $p<0.0001$.

Results

Mechanical stiffness of HCC cells is inversely correlated with their motility

Tumor cells dynamically alter their mechanical properties during tumor progression [29-31]. In order to explore the relationship between mechanical stiffness and motility,

HCC cells with different malignancy (MHCC97-L and HepG2) were utilized for the measurement of their stiffness by AFM. Young's modulus was used to describe cellular stiffness and calculated by fitting the force-indentation curve of each measurement using the Hertzian contact model. The measurement results showed that MHCC97-L cells exhibited higher stiffness (3.74 ± 0.15 kPa; Figure 1a) compared to HepG2 cells (2.82 ± 0.11 kPa). The histograms of the stiffness distribution indicated the obvious shift of the mean stiffness of HepG2 to the lower side compared to MHCC97-L (Figure 1a). It has been reported that actin filament network is a crucial cytoskeletal component that determines cellular stiffness [32]. Therefore, F-actin and phosphorylation of myosin light chain (pMLC) were measured by immunofluorescence staining in these HCC cells. The levels of both F-actin and pMLC notably decreased in HepG2 cells compared to MHCC97-L (Figure 1b), which might explain the reduction in cellular stiffness of these cells. Further, the migration and invasion of these HCC cells were examined. MHCC97-L cells exhibited lower wound healing, Transwell migration, and 3D Matrigel invasion ability than HepG2 (Figure 1c-e). All these data demonstrate that mechanical stiffness of HCC cells is inversely correlated with their migration and invasion ability.

Reducing actomyosin activity softens HCC cells and promotes migration and invasion

We have established the inverse correlation between cellular stiffness and motility in HCC cells. However, it is still unknown whether the alteration of mechanical stiffness in tumor progression influences HCC cell migration and invasion. To answer this question, the mechanical properties of tumor cells were modulated by targeting actomyosin activity, as cellular stiffness is mainly determined by actin cytoskeleton and ROCK/MLCK/myosin-mediated contractility [33-36]. ROCK inhibitor Y-27632 and

myosin II inhibitor Blebbistatin (Bleb) were adopted to pre-treat HCC cells for different durations and the influence on cellular functions was examined. The experimental conditions were optimized so that such treatment had no obvious cytotoxicity but significantly affected cell motility (Supplementary Figure 1a-g). The pharmacologic pre-treatment lowered down F-actin level, F-actin/G-actin ratio, and pMLC (Figure 2a and 2b), indicating the reduction of actomyosin activity. HCC cellular stiffness was reduced by ~30% after the treatment of Y-27632 and Bleb (Figure 2b). The effects of such pre-treatment on the migration and invasion of HCC cells were then investigated. The results showed that the migratory capacity of HepG2 cells was significantly elevated after the treatment of Y-27632 and Bleb (Figure 2c-e). Y-27632 also enhanced the migration of Huh-7 cells (Supplementary Figure 1h, i). Furthermore, the invasive potential, as measured by Transwell invasion assay and 3D tumor spheroid invasion assay, showed a significant increase after the treatment of Bleb and Y-27632 (Figure 2f, g). Note that the 3D invasion assay was conducted in low serum medium and the modulation of cellular stiffness had minimal influence on cell proliferation (Supplementary Figure 1a, 2f, 3a, and 4d). Therefore, the effect of cell proliferation on tumor cell invasion could be excluded. In addition, the stiffness measurement by AFM was conducted on two dimensional substrates, which might not correlate well to cell behavior in three dimensional matrices.

We further modified tumor cell mechanics by genetically knocking down mDia1, an essential downstream effector of RhoA and a major contributor for F-actin polymerization [37, 38], and MLCK, a key regulator of myosin II activity. Silencing these genes decreased the levels of pMLC and F-actin (Supplementary Figure 2a-d). Compared to control cells, knocking down MLCK or mDia1 reduced cellular stiffness but did not influence cell proliferation and morphology (Figure 2h; Supplementary Figure 2e-i). Remarkably, silencing MLCK or mDia1 facilitated wound healing and cell

migration in Transwell assay (Figure 2i-k) and tumor cell invasion in the Matrigel invasion assay (Figure 2j, l). During the metastatic process, tumor cells secrete matrix metalloproteinases (MMPs) to degrade extracellular matrix (ECM) components, which can favor tumor cell invasion [39, 40]. We then examined the mRNA expression of MMP9, one of the key members in MMP family. Silencing mDia1 and MLCK enhanced MMP9 expression by 15- and 5-fold, respectively (Supplementary Figure 2j). In addition, the influence of altering cell mechanics on motility was tested in another HCC cell line. Consistently, the inhibition of MLCK or mDia1 significantly enhanced cell migration and invasion in MHCC97-L cells (Supplementary Figure 2k-n).

Taken together, these findings suggest that inhibiting actomyosin activity decreases cellular stiffness but promotes HCC migration and invasion.

Activating actomyosin stiffens HCC cells and impairs migration and invasion

Our results have shown that lowering actomyosin activity leads to reduced cellular stiffness but enhanced migration and invasion in HCC cells, suggesting that cell softening may be sufficient to promote motility. On the contrary, we further explored whether low actomyosin and cellular stiffness were required to sustain such ability. Jasplakinolide (Jasp) and Narciclasine (Narci) were utilized to strengthen the cytoskeleton through facilitating F-actin polymerization and Rho activation. The pharmacologic pre-treatment enhanced F-actin level, F-actin/G-actin ratio, and pMLC (Figure 3a and 3b) but did not influence the proliferation of HepG2 cells (Supplementary Figure 3a). Cellular stiffness was increased by ~20% after the treatment of Jasp and Narci (Figure 3b). Notably, such treatment obviously reduced the migration (by 20-43%) and Transwell invasion (by 33-39%) of HepG2 cells (Figure 3c-e). Strengthening the cytoskeleton significantly decreased tumor cell invasion by ~40% in 3D collagen gels (Figure 3f). Further, the inhibitory effect of cytoskeletal stiffening

on motility was also observed in another HCC cell line MHCC97-L (Supplementary Figure 3b-e), suggesting that the influence of actomyosin activity on tumor cell motility may be not cell line dependent.

To modulate the ROCK/MLCK/myosin activity specifically, we overexpressed constitutively active (CA) forms of MLCK and ROCK mutants in HepG2 cells, which could enhance myosin activity and cellular stiffness [41]. Indeed, CA plasmids increased the levels of pMLC and F-actin but had no obvious suppressive effect on cell proliferation and morphology (Supplementary Figure 4a-g). Overexpressing CA-MLCK or CA-ROCK in HepG2 cells increased cellular stiffness from 2.39 ± 0.086 kPa in the control group to 3.29 ± 0.14 kPa in CA-MLCK group and 3.74 ± 0.21 kPa in CA-ROCK group (Figure 3g). After such treatment, the distribution of cell stiffness became broader, and the peak value shifted to the higher side (Supplementary Figure 4c). Further, the effects of CA plasmids on the motility were examined. Activating myosin obviously inhibited wound healing (Figure 3h), Transwell migration (Figure 3i, j), and invasion (Figure 3i, k). The expressions of MMP2 and MMP9 were found to be reduced after the treatment (Supplementary Figure 4h), indicating the impaired invasive potential. In addition, strengthening cytoskeleton suppressed migration and invasion in another HCC cell line Huh-7 (Supplementary Figure 4i-k).

In summary, these results demonstrate that elevating actomyosin activity increases cellular stiffness but inhibits tumor cell migration and invasion.

Actomyosin regulates the motility of HCC cells through the effect on cellular stiffness

Our findings have demonstrated that enhancing/reducing actomyosin activity suppresses/promotes the migration and invasion of HCC cells. We further tested whether the influence of actomyosin on motility was through the effect on cell

mechanics. Towards this goal, MLCK was silenced in HepG2 cells with siRNA and then re-expressed with CA-MLCK plasmids. Consistently, inhibiting MLCK reduced cellular stiffness but promoted both migratory and invasion ability, which were rescued to the control levels after overexpression of MLCK (Figure 4a-c). It is known that MLCK and ROCK increase the mono- and di-phosphorylation of the regulatory light chain of myosin II, respectively, thereby facilitating the interaction between actin and myosin II that strengthens the cytoskeleton and increases cellular stiffness [42]. We then asked whether MLCK and ROCK influence HCC cell motility through the effect on cell mechanics. HCC cells were overexpressed with CA-MLCK and CA-ROCK plasmids and then treated with Bleb or Cytochalasin D (CytoD), which can inhibit myosin activity or disrupt actin cytoskeleton. The results showed that overexpression of CA-MLCK and CA-ROCK significantly suppressed the migration and invasion ability of HCC cells, which were restored to the control levels after the treatment of Bleb or CytoD (Figure 4d-i). Further, HepG2 cells were transfected with the siRNAs of MLCK and mDia1 and then treated with Jasp. In consistent, silencing MLCK and mDia1 enhanced both migratory and invasion ability (Figure 4j-l), which was then diminished by the treatment of Jasp. All these findings suggest that actomyosin-mediated cellular stiffness regulates the motility of HCC cells.

Actomyosin-mediated cellular stiffness regulates the migration and invasion through JNK signaling

JNK belongs to the mitogen-activated protein kinases (MAPKs) family. MAPK and JNK signaling are responsive to various mechanical stimuli [43-45] and involved in tumor metastasis [46-48]. Recent evidence shows that there is a feedback loop among JNK, RhoA, and F-actin remodeling [49] and phosphorylated JNK is increased when MLCK is lost in breast cancer [50], suggesting that the activation of JNK signaling is

related to cytoskeleton [51]. We thus hypothesized that cellular stiffness regulated HCC cell migration and invasion through JNK signaling. To test this hypothesis, we first examined the influence of cell mechanics on JNK activity. Softening HCC cells down-regulated the expressions of the upstream genes MKK4 and MKK7 that could directly activate JNK (Figure 5a) [52] and reduced the phosphorylated but not total amounts of JNK1 and JNK2 (Figure 5c; Supplementary Figure 5a). On the other hand, stiffening cells up-regulated MKK4 and MKK7 and promoted the phosphorylated amount of JNK (Figure 5b, c; Supplementary Figure 5a). However, Anisomycin, a JNK activator, did not influence cellular stiffness (Supplementary Figure 5h, i). These results suggest that actomyosin-mediated cellular stiffness significantly suppresses the activity of JNK signaling, while JNK activation has no obvious effect on cell mechanics.

Further, we explored the roles of JNK signaling in mediating the effect of cellular stiffness on tumor cell motility. Softening HCC cells increased the migration and invasion of HepG2 and Huh-7 cells (Figure 5d-f; Supplementary Figure 5b-d), which was abolished by the simultaneous activation of JNK signaling. Interestingly, the activation of JNK increased the migration and invasion of control Huh-7 but not HepG2 cells while reducing the motility of softened HCC cells to the control level (Supplementary Figure 5b-d). On the other hand, stiffening cells decreased the migration and invasion of HepG2 and Huh-7 cells, which were rescued to the similar levels of control cells after the treatment of JNK inhibitor SP600125 (Figure 5g-i; Supplementary Figure 5e-g). Note that inhibition of JNK signaling affected cell migration but not invasion in control HCC cells and dramatically increased the migration and invasion of the stiffened cells.

In summary, all these findings conclude that cellular stiffness regulates HCC cell migration and invasion through JNK signaling.

Stiffening HCC CSCs reduces migration and invasion through elevating JNK phosphorylation

Compared to conventional cancer cells, CSCs drive tumor progression and pose a serious challenge to cancer therapy due to the high malignancy, drug resistance, and metastatic potential [53]. CSCs are believed to be the seeds of tumor metastasis and usually show reduced cellular stiffness [54-56]. Therefore, we wondered whether low cellular stiffness of CSCs could be a potential target for the inhibition of motility. To test this idea, CSCs were obtained by culturing HCC cells in 90-Pa 3D soft fibrin gels [55]. Indeed, HCC CSCs had lower mechanical stiffness and F-actin but higher migration and invasion ability compared to non-CSCs (Figure 6a-e). These malignant tumor cells exhibited reduced level of phosphorylated JNK (Figure 6e). Activating JNK signaling in CSCs notably decreased their migration and invasion ability to the levels of non-CSCs (Figure 6f-h), indicating the indispensable role of low JNK activity in CSC's motility. Further, overexpressing CA-MLCK and CA-ROCK plasmids significantly increased the stiffness of CSCs from 2.36 ± 0.13 kPa to 3.94 ± 0.23 kPa and 3.20 ± 0.19 kPa, respectively (Figure 6i; Supplementary Figure 5j). As a result, stiffening CSCs dramatically impaired their migration and invasion ability by 34-49% and 76-89%, respectively (Figure 6j-l). These results suggest that cellular stiffening significantly inhibits the motility of HCC CSCs.

Furthermore, we explored the role of JNK signaling in cellular stiffness-induced reduction in CSC migration and invasion. The overexpression of CA-MLCK and CA-ROCK increased F-actin polymerization (Figure 6m, o), supporting the elevation in the stiffness of CSCs. On the other hand, CSC stiffening promoted JNK phosphorylation, suggesting the activation of this signaling (Figure 6m, n). Consistently, stiffening CSCs by CA-MLCK or CA-ROCK considerably reduced the migration and invasion, which were rescued by the simultaneous inhibition of JNK signaling (Figure 6p-r). These

findings demonstrate that cellular stiffening inhibits CSC motility through activating JNK phosphorylation.

Discussion

Mechanical cues play pivotal roles at different metastatic stages [57-59], where cancer cells dynamically remodel cytoskeleton structures and alter their mechanical properties. Mechanical stiffness of cancer cells has been proposed to grade their malignancy, including stemness, tumorigenicity, and metastatic potential [18, 20, 23]. In particular, highly metastatic cells exhibit low stiffness and high deformability [22, 60-62]. This study not only establishes the inverse correlation between mechanical stiffness of HCC cells and their motility, but more importantly deciphers the regulatory role of cell mechanics in tumor cell migration and invasion. Specifically, weakening HCC cells promotes their motility, suggesting that cell softening during tumor progression may be sufficient to facilitate the motile phenotype and thus could be a driving force for metastasis. On the other hand, strengthening tumor cells impairs their motility, implicating the indispensability of low cellular stiffness in sustaining high metastatic competence. Consistently, it has been reported that 4-hydroxyacetophenone that targets myosin IIC activity alters actin cytoskeleton organization and enhances actomyosin-mediated contractility while effectively inhibiting metastatic competence of pancreatic and colon cancer [63, 64].

This study alters cellular mechanics by pharmacologically and genetically modulating myosin activity and actin cytoskeleton. It is known that targeting actomyosin not only alters cell mechanics, but also may influence other cell functions [33, 65, 66]. To alleviate this potential off-target issue, we have chosen moderate doses of drugs, siRNAs, and CA plasmids to minimize the potential influence on cell morphology, viability, and proliferation. Importantly, the suppressive effect of tumor cell stiffening

through activating ROCK/MLCK/myosin signaling on migration and invasion can be rescued by the disruption of F-actin cytoskeleton. Further, the promotive effect of cell softening through silencing MLCK is diminished by the activation of F-actin polymerization. These findings suggest that the observed influence of actomyosin activity on tumor cell motility is probably through the effect on cell mechanics. Nevertheless, identifying new targets that are "only" or closely related to cellular stiffness or altering cell mechanical properties through other means will further validate the roles of tumor cell mechanics in malignancy. Therefore, the mechanical regulation of cell motility implicates the potential therapeutic roles of cellular mechanics in suppressing tumor metastasis. CSCs are commonly regarded as one critical seed of metastasis in various types of cancer and exhibit unique mechanical signature [67]. Our previous work together with many others reports that CSCs display much lower stiffness than non-CSCs in skin, breast, and ovarian cancer [24, 55, 68]. Recent evidence shows that overexpressing capping protein-inhibiting regulator of actin dynamics in colon tumor-repopulating cells strengthens F-actin cytoskeleton and reduces their stemness and metastasis [69]. Indeed, we show that HCC CSCs are more migratory and invasive but much softer than non-CSCs. Stiffening these CSCs through overexpression of MLCK and ROCK considerably inhibits their motility, suggesting the potential of cellular stiffness as a promising therapeutic target for the prevention of metastasis.

It has been long recognized that JNK signaling is stress-activated and plays both oncogenic and tumor suppressive roles in metastasis [70, 71]. Many studies report that JNK signaling can be activated to accelerate HCC metastasis in response to various stimuli and upstream signaling [72, 73]. In contrast, recent evidence shows that inhibition of JNK phosphorylation and nuclear translocation promotes the formation of lamellipodium, which contributes to HCC invasion [74]. WZ35, a derivative of anti-

cancer drug curcumin, suppresses HCC metastasis by promoting ROS-dependent JNK activation [75]. A triazolothiadiazine derivative induces HCC cell death and inhibits motility through the activation of JNK signaling [76]. The roles of JNK in HCC are further complicated by the findings that lack of JNK in hepatocytes facilitates HCC tumorigenesis while suppressing the inflammation and HCC development [77]. Further, JNK signaling is not only crucial in maintaining the integrity and functions of cytoskeleton, but also affected by cytoskeleton dynamics [49, 78, 79]. The reciprocity among RhoA, JNK signaling, and F-actin cytoskeleton influences tumor cell migration and invasion [49, 51]. Of note, the knockdown of MLCK promotes breast cancer migration but activates JNK signaling, while the inhibition of the kinase function of MLCK suppresses cell motility [80], indicating the distinct functions of catalytic and scaffolding MLCK. It will be worthy to further explore the effects of these two MLCK functions on HCC cell mechanics, JNK activity, and metastasis in the future. Nevertheless, it is not too surprising that the mechanics of cytoskeleton can affect JNK signaling and further tumor metastasis. This study shows that cell weakening/strengthening reduces/promotes JNK activation, which then enhances/suppresses HCC cell motility. Further, stiffening HCC CSCs attenuates their migration and invasion through JNK phosphorylation. Therefore, our findings suggest that tumor cell softening during tumor progression facilitates HCC metastasis via the suppression of JNK signaling, which may add another layer of complexity to the role of JNK in HCC that should be carefully re-considered in cancer therapeutics.

Epithelial-mesenchymal transition is critical in tumor metastasis and accompanied by the alterations in the mechanical properties of tumor cells, such as cellular stiffness, cell-ECM adhesion, and cell-cell adhesion [24, 81]. For example, highly migratory tumor cells are usually less stiff, more mesenchymal [23], and have lower cell-ECM adhesion strength compared to weakly malignant cells [82]. The leader cells in the front

of collective cell migration are much softer and exhibit reduced adhesion force than the follower cells within the cell clusters [83, 84]. These leader cells downregulate epithelial markers and upregulate mesenchymal markers, especially Snail and Vimentin. The treatment of cancer cells with cyclosporine or TGF-β induces EMT, which leads to the reduction of cellular stiffness and increase of migration ability and stemness [85]. Further, cell-cell adhesion is crucial in collective cell migration and mainly mediated by cadherins [86]. In particular, loss of E-cadherin is one feature of EMT and can reduce cellular stiffness, cell-cell adhesion, and cancer cell proliferation. Therefore, our results together with these findings suggest that the mechanics of tumor cells alter during tumor progression (e.g., EMT), such as cytoskeletal rearrangement, tumor cell softening, and reduction of cell-ECM and cell-cell adhesion, which may collectively contribute to metastasis. This idea warrants further investigation in the future, which will provide new evidence to elucidate the roles of tumor cell mechanics in cancer.

In addition to the reduction of cell stiffness, tumor tissues become stiffened during progression, i.e., the rigidity of the entire tumors increases due to excessive deposition of ECM proteins (e.g., collagen) and enhanced crosslinking [81, 87]. Many reports have shown that stiff tumor tissues facilitate metastasis by promoting local migration and invasion [88], intravasation [89], extravasation [90], and metastatic colonization [91]. On the other hand, *in vitro* culture of tumor cells on stiff matrices elevates the formation of stress fibers and myosin activation and thus increase cellular contractility and stiffness [92], which may reduce tumor metastasis according to our findings. However, this presumption is not consistent with the promotive effect of stiff tissues on metastasis. A recent study has attempted to address this paradox of the co-existence of soft tumor cells and stiff tumor tissues [93], reporting that primary tumors are mechanically heterogeneous from the cell to tissue level. Soft tumor cells promote the unjamming phenomenon and thus assume a motile phenotype within cell clusters, while increase in

cellular stiffness arrests them in jammed regions and reduces cell motility. Yet, whether and how the mechanics of tumor tissues and tumor cells synergistically or independently influence tumor metastasis remain incompletely understood.

Conclusion

This study reports that the stiffness of HCC cells not only correlates with but also regulates their migration and invasion. In particular, weakening cell cytoskeleton by the inhibition of actomyosin decreases cellular stiffness but promotes tumor cell motility, while strengthening HCC cells increases mechanical stiffness but inhibits such ability. The regulation of migration and invasion by actomyosin activity is through the effect on cell mechanics. Mechanistically, softening/stiffening HCC cells inhibits/promotes JNK phosphorylation, activation/inhibition of which can abolish the effect of cellular mechanics on cell motility. Furthermore, stiffening HCC CSCs significantly inhibits their motility through activating JNK signaling. In conclusion, this study reveals that actomyosin-mediated cellular stiffness regulates tumor cell migration and invasion via governing JNK signaling in HCC and identifies the therapeutic potential of cell mechanics as a promising target for cancer mechanotargeting.

Acknowledgements

We thank the University Life Science Facility in the Hong Kong Polytechnic University for providing the confocal laser scanning microscopy, flow cytometry, and central animal facility. We acknowledge the support from National Natural Science Foundation of China (Project no. 11972316), Shenzhen Science and Technology Innovation Commission (Project no. JCYJ20200109142001798, SGDX2020110309520303, and

JCYJ20220531091002006), General Research Fund of Hong Kong Research Grant Council (PolyU 15214320 and 15227523), Health and Medical Research Fund (18191421), and the internal grant from the Hong Kong Polytechnic University (1-ZE2M, 1-CD75, and 1-ZVY1).

Competing Interests

The authors declare no competing financial interest.

Supplementary Material

The Supplementary material includes 5 supplementary figures and 1 table.

Reference

[1] P. Mehlen, A. Puisieux, Metastasis: a question of life or death, Nat Rev Cancer 6(6) (2006) 449-58.
[2] A.W. Lambert, D.R. Pattabiraman, R.A. Weinberg, Emerging Biological Principles of Metastasis, Cell 168(4) (2017) 670-691.
[3] A. Aguayo, Y.Z. Patt, Nonsurgical treatment of hepatocellular carcinoma, Semin Oncol 28(5) (2001) 503-13.
[4] S. Valastyan, R.A. Weinberg, Tumor metastasis: molecular insights and evolving paradigms, Cell 147(2) (2011) 275-92.
[5] J. Fares, M.Y. Fares, H.H. Khachfe, H.A. Salhab, Y. Fares, Molecular principles of metastasis: a hallmark of cancer revisited, Signal Transduct Target Ther 5(1) (2020) 28.
[6] S. Shen, S. Vagner, C. Robert, Persistent Cancer Cells: The Deadly Survivors, Cell 183(4) (2020) 860-874.
[7] A. Forner, M. Reig, J. Bruix, Hepatocellular carcinoma, Lancet 391(10127) (2018) 1301-1314.
[8] S. Kumar, V.M. Weaver, Mechanics, malignancy, and metastasis: the force journey of a tumor cell, Cancer Metastasis Rev 28(1-2) (2009) 113-27.
[9] F. Broders-Bondon, T.H. Nguyen Ho-Bouldoires, M.E. Fernandez-Sanchez, E. Farge, Mechanotransduction in tumor progression: The dark side of the force, J Cell Biol 217(5) (2018) 1571-1587.
[10] A. Malandrino, R.D. Kamm, E. Moeendarbary, In Vitro Modeling of Mechanics in Cancer Metastasis, ACS Biomater Sci Eng 4(2) (2018) 294-301.

[11] S. Suresh, Biomechanics and biophysics of cancer cells, Acta Biomater 3(4) (2007) 413-38.
[12] S.E. Cross, Y.S. Jin, J. Rao, J.K. Gimzewski, Nanomechanical analysis of cells from cancer patients, Nat Nanotechnol 2(12) (2007) 780-3.
[13] Q.S. Li, G.Y. Lee, C.N. Ong, C.T. Lim, AFM indentation study of breast cancer cells, Biochem Biophys Res Commun 374(4) (2008) 609-13.
[14] S.M. Seyedpour, M. Pachenari, M. Janmaleki, M. Alizadeh, H. Hosseinkhani, Effects of an antimitotic drug on mechanical behaviours of the cytoskeleton in distinct grades of colon cancer cells, J Biomech 48(6) (2015) 1172-8.
[15] M. Lekka, P. Laidler, D. Gil, J. Lekki, Z. Stachura, A.Z. Hrynkiewicz, Elasticity of normal and cancerous human bladder cells studied by scanning force microscopy, European biophysics journal : EBJ 28(4) (1999) 312-6.
[16] M.E. Grady, R.J. Composto, D.M. Eckmann, Cell elasticity with altered cytoskeletal architectures across multiple cell types, J Mech Behav Biomed Mater 61 (2016) 197-207.
[17] M. Plodinec, M. Loparic, C.A. Monnier, E.C. Obermann, R. Zanetti-Dallenbach, P. Oertle, J.T. Hyotyla, U. Aebi, M. Bentires-Alj, R.Y. Lim, C.A. Schoenenberger, The nanomechanical signature of breast cancer, Nat Nanotechnol 7(11) (2012) 757-65.
[18] J. Lv, Y. Liu, F. Cheng, J. Li, Y. Zhou, T. Zhang, N. Zhou, C. Li, Z. Wang, L. Ma, M. Liu, Q. Zhu, X. Liu, K. Tang, J. Ma, H. Zhang, J. Xie, Y. Fang, H. Zhang, N. Wang, Y. Liu, B. Huang, Cell softness regulates tumorigenicity and stemness of cancer cells, Embo j 40(2) (2021) e106123.
[19] J. Chen, W. Zhou, Q. Jia, J. Chen, S. Zhang, W. Yao, F. Wei, Y. Zhang, F. Yang, W. Huang, Y. Zhang, H. Zhang, Y. Zhang, B. Huang, Z. Zhang, H. Jia, N. Wang, Efficient extravasation of tumor-repopulating cells depends on cell deformability, Sci Rep 6 (2016) 19304.
[20] H. Ohata, T. Ishiguro, Y. Aihara, A. Sato, H. Sakai, S. Sekine, H. Taniguchi, T. Akasu, S. Fujita, H. Nakagama, K. Okamoto, Induction of the stem-like cell regulator CD44 by Rho kinase inhibition contributes to the maintenance of colon cancer-initiating cells, Cancer Res 72(19) (2012) 5101-10.
[21] D.J. Castro, J. Maurer, L. Hebbard, R.G. Oshima, ROCK1 inhibition promotes the self-renewal of a novel mouse mammary cancer stem cell, Stem Cells 31(1) (2013) 12-22.
[22] V. Swaminathan, K. Mythreye, E.T. O'Brien, A. Berchuck, G.C. Blobe, R. Superfine, Mechanical stiffness grades metastatic potential in patient tumor cells and in cancer cell lines, Cancer Res 71(15) (2011) 5075-80.
[23] W. Xu, R. Mezencev, B. Kim, L. Wang, J. McDonald, T. Sulchek, Cell stiffness is a biomarker of the metastatic potential of ovarian cancer cells, PLoS One 7(10) (2012)

e46609.
[24] X. Chen, K. Tang, X. Li, C. Zhang, Y. Xin, K. Li, Y. Tan, Biomechanics of cancer stem cells, Essays Biochem 66(4) (2022) 359-369.
[25] V. Gensbittel, M. Kräter, S. Harlepp, I. Busnelli, J. Guck, J.G. Goetz, Mechanical Adaptability of Tumor Cells in Metastasis, Dev Cell 56(2) (2021) 164-179.
[26] Y. Xin, X. Chen, X. Tang, K. Li, M. Yang, W.C. Tai, Y. Liu, Y. Tan, Mechanics and Actomyosin-Dependent Survival/Chemoresistance of Suspended Tumor Cells in Shear Flow, Biophys J 116(10) (2019) 1803-1814.
[27] E.K. Dimitriadis, F. Horkay, J. Maresca, B. Kachar, R.S. Chadwick, Determination of elastic moduli of thin layers of soft material using the atomic force microscope, Biophysical journal 82(5) (2002) 2798-810.
[28] S. Kontomaris, A. Stylianou, K. Nikita, A.J.M.R.E. Malamou, Determination of the linear elastic regime in AFM nanoindentation experiments on cells, 6(11) (2019) 115410.
[29] A.F. Pegoraro, P. Janmey, D.A. Weitz, Mechanical Properties of the Cytoskeleton and Cells, Cold Spring Harb Perspect Biol 9(11) (2017).
[30] Y. Abidine, V.M. Laurent, R. Michel, A. Duperray, C. Verdier, Local mechanical properties of bladder cancer cells measured by AFM as a signature of metastatic potential, The European Physical Journal Plus 130(10) (2015) 202.
[31] C.N. Holenstein, A. Horvath, B. Schär, A.D. Schoenenberger, M. Bollhalder, N. Goedecke, G. Bartalena, O. Otto, M. Herbig, J. Guck, D.A. Müller, J.G. Snedeker, U. Silvan, The relationship between metastatic potential and in vitro mechanical properties of osteosarcoma cells, Mol Biol Cell 30(7) (2019) 887-898.
[32] L. Blanchoin, R. Boujemaa-Paterski, C. Sykes, J. Plastino, Actin dynamics, architecture, and mechanics in cell motility, Physiol Rev 94(1) (2014) 235-63.
[33] D.A. Fletcher, R.D. Mullins, Cell mechanics and the cytoskeleton, Nature 463(7280) (2010) 485-92.
[34] N. Gavara, R.S. Chadwick, Relationship between cell stiffness and stress fiber amount, assessed by simultaneous atomic force microscopy and live-cell fluorescence imaging, Biomech Model Mechanobiol 15(3) (2016) 511-23.
[35] S. Sen, S. Kumar, Cell-Matrix De-Adhesion Dynamics Reflect Contractile Mechanics, Cell Mol Bioeng 2(2) (2009) 218-230.
[36] S. Vichare, S. Sen, M.M. Inamdar, Cellular mechanoadaptation to substrate mechanical properties: contributions of substrate stiffness and thickness to cell stiffness measurements using AFM, Soft Matter 10(8) (2014) 1174-81.
[37] P. Hotulainen, P. Lappalainen, Stress fibers are generated by two distinct actin assembly mechanisms in motile cells, J Cell Biol 173(3) (2006) 383-94.
[38] A. Kostic, M.P. Sheetz, Fibronectin rigidity response through Fyn and p130Cas

recruitment to the leading edge, Mol Biol Cell 17(6) (2006) 2684-95.
[39] S. Niland, A.X. Riscanevo, J.A. Eble, Matrix Metalloproteinases Shape the Tumor Microenvironment in Cancer Progression, Int J Mol Sci 23(1) (2021).
[40] L. Liu, Y. Ye, X. Zhu, MMP-9 secreted by tumor associated macrophages promoted gastric cancer metastasis through a PI3K/AKT/Snail pathway, Biomed Pharmacother 117 (2019) 109096.
[41] S.Y. Wong, T.A. Ulrich, L.P. Deleyrolle, J.L. MacKay, J.M. Lin, R.T. Martuscello, M.A. Jundi, B.A. Reynolds, S. Kumar, Constitutive activation of myosin-dependent contractility sensitizes glioma tumor-initiating cells to mechanical inputs and reduces tissue invasion, Cancer Res 75(6) (2015) 1113-22.
[42] E. Kassianidou, J.H. Hughes, S. Kumar, Activation of ROCK and MLCK tunes regional stress fiber formation and mechanics via preferential myosin light chain phosphorylation, Mol Biol Cell 28(26) (2017) 3832-3843.
[43] S. Li, M. Kim, Y.L. Hu, S. Jalali, D.D. Schlaepfer, T. Hunter, S. Chien, J.Y. Shyy, Fluid shear stress activation of focal adhesion kinase. Linking to mitogen-activated protein kinases, J Biol Chem 272(48) (1997) 30455-62.
[44] Y. Xin, K. Li, M. Yang, Y. Tan, Fluid Shear Stress Induces EMT of Circulating Tumor Cells via JNK Signaling in Favor of Their Survival during Hematogenous Dissemination, Int J Mol Sci 21(21) (2020).
[45] T.V. Nguyen, M. Sleiman, T. Moriarty, W.G. Herrick, S.R. Peyton, Sorafenib resistance and JNK signaling in carcinoma during extracellular matrix stiffening, Biomaterials 35(22) (2014) 5749-59.
[46] A.S. Dhillon, S. Hagan, O. Rath, W. Kolch, MAP kinase signalling pathways in cancer, Oncogene 26(22) (2007) 3279-90.
[47] H. Noguchi, Regulation of c-Jun NH(2)-Terminal Kinase for Islet Transplantation, J Clin Med 8(11) (2019).
[48] J. Wang, I. Kuiatse, A.V. Lee, J. Pan, A. Giuliano, X. Cui, Sustained c-Jun-NH2-kinase activity promotes epithelial-mesenchymal transition, invasion, and survival of breast cancer cells by regulating extracellular signal-regulated kinase activation, Mol Cancer Res 8(2) (2010) 266-77.
[49] V.A. Rudrapatna, E. Bangi, R.L. Cagan, A Jnk-Rho-Actin remodeling positive feedback network directs Src-driven invasion, Oncogene 33(21) (2014) 2801-6.
[50] D.Y. Kim, D.M. Helfman, Loss of MLCK leads to disruption of cell-cell adhesion and invasive behavior of breast epithelial cells via increased expression of EGFR and ERK/JNK signaling, Oncogene 35(34) (2016) 4495-508.
[51] B. Benoit, A. Baillet, C. Poüs, Cytoskeleton and Associated Proteins: Pleiotropic JNK Substrates and Regulators, Int J Mol Sci 22(16) (2021).
[52] W. Haeusgen, T. Herdegen, V. Waetzig, The bottleneck of JNK signaling:

molecular and functional characteristics of MKK4 and MKK7, Eur J Cell Biol 90(6-7) (2011) 536-44.
[53] E.K. Ramos, A.D. Hoffmann, S.L. Gerson, H. Liu, New Opportunities and Challenges to Defeat Cancer Stem Cells, Trends Cancer 3(11) (2017) 780-796.
[54] A.Z. Ayob, T.S. Ramasamy, Cancer stem cells as key drivers of tumour progression, J Biomed Sci 25(1) (2018) 20.
[55] J. Liu, Y. Tan, H. Zhang, Y. Zhang, P. Xu, J. Chen, Y.C. Poh, K. Tang, N. Wang, B. Huang, Soft fibrin gels promote selection and growth of tumorigenic cells, Nat Mater 11(8) (2012) 734-41.
[56] D. Thomas, P.S. Thiagarajan, V. Rai, O. Reizes, J. Lathia, T. Egelhoff, Increased cancer stem cell invasion is mediated by myosin IIB and nuclear translocation, Oncotarget 7(30) (2016) 47586-47592.
[57] F.M. White, R.A. Gatenby, C. Fischbach, The Physics of Cancer, Cancer Res 79(9) (2019) 2107-2110.
[58] G.P. Gupta, J. Massagué, Cancer metastasis: building a framework, Cell 127(4) (2006) 679-95.
[59] A.V. Nguyen, K.D. Nyberg, M.B. Scott, A.M. Welsh, A.H. Nguyen, N. Wu, S.V. Hohlbauch, N.A. Geisse, E.A. Gibb, A.G. Robertson, T.R. Donahue, A.C. Rowat, Stiffness of pancreatic cancer cells is associated with increased invasive potential, Integr Biol (Camb) 8(12) (2016) 1232-1245.
[60] S.E. Cross, Y.S. Jin, J. Tondre, R. Wong, J. Rao, J.K. Gimzewski, AFM-based analysis of human metastatic cancer cells, Nanotechnology 19(38) (2008) 384003.
[61] J. Fenner, A.C. Stacer, F. Winterroth, T.D. Johnson, K.E. Luker, G.D. Luker, Macroscopic stiffness of breast tumors predicts metastasis, Sci Rep 4 (2014) 5512.
[62] T. Watanabe, H. Kuramochi, A. Takahashi, K. Imai, N. Katsuta, T. Nakayama, H. Fujiki, M. Suganuma, Higher cell stiffness indicating lower metastatic potential in B16 melanoma cell variants and in (-)-epigallocatechin gallate-treated cells, J Cancer Res Clin Oncol 138(5) (2012) 859-66.
[63] A. Surcel, E.S. Schiffhauer, D.G. Thomas, Q. Zhu, K.T. DiNapoli, M. Herbig, O. Otto, H. West-Foyle, A. Jacobi, M. Kräter, K. Plak, J. Guck, E.M. Jaffee, P.A. Iglesias, R.A. Anders, D.N. Robinson, Targeting Mechanoresponsive Proteins in Pancreatic Cancer: 4-Hydroxyacetophenone Blocks Dissemination and Invasion by Activating MYH14, Cancer Res 79(18) (2019) 4665-4678.
[64] D.S. Bryan, M. Stack, K. Krysztofiak, U. Cichoń, D.G. Thomas, A. Surcel, E.S. Schiffhauer, M.A. Beckett, N.N. Khodarev, L. Xue, E.C. Poli, A.T. Pearson, M.C. Posner, D.N. Robinson, R.S. Rock, R.R. Weichselbaum, 4-Hydroxyacetophenone modulates the actomyosin cytoskeleton to reduce metastasis, Proc Natl Acad Sci U S A 117(36) (2020) 22423-22429.

[65] S. Seetharaman, S. Etienne-Manneville, Cytoskeletal Crosstalk in Cell Migration, Trends Cell Biol 30(9) (2020) 720-735.
[66] C. Ruggiero, E. Lalli, Targeting the cytoskeleton against metastatic dissemination, Cancer Metastasis Rev 40(1) (2021) 89-140.
[67] A. Roy Choudhury, S. Gupta, P.K. Chaturvedi, N. Kumar, D. Pandey, Mechanobiology of Cancer Stem Cells and Their Niche, Cancer Microenviron 12(1) (2019) 17-27.
[68] X. Chen, Y. Fan, J. Sun, Z. Zhang, Y. Xin, K. Li, K. Tang, P. Du, Y. Liu, G. Wang, M. Yang, Y. Tan, Nanoparticle-mediated specific elimination of soft cancer stem cells by targeting low cell stiffness, Acta Biomater 135 (2021) 493-505.
[69] Y. Chang, J. Zhang, X. Huo, X. Qu, C. Xia, K. Huang, F. Xie, N. Wang, X. Wei, Q. Jia, Substrate rigidity dictates colorectal tumorigenic cell stemness and metastasis via CRAD-dependent mechanotransduction, Cell Rep 38(7) (2022) 110390.
[70] M. Enomoto, D. Kizawa, S. Ohsawa, T. Igaki, JNK signaling is converted from anti- to pro-tumor pathway by Ras-mediated switch of Warts activity, Dev Biol 403(2) (2015) 162-71.
[71] S.Y. Tam, H.K. Law, JNK in Tumor Microenvironment: Present Findings and Challenges in Clinical Translation, Cancers (Basel) 13(9) (2021).
[72] J. Wang, G. Tai, Role of C-Jun N-terminal Kinase in Hepatocellular Carcinoma Development, Target Oncol 11(6) (2016) 723-738.
[73] L. Min, B. He, L. Hui, Mitogen-activated protein kinases in hepatocellular carcinoma development, Semin Cancer Biol 21(1) (2011) 10-20.
[74] C. Shi, Y. Cai, Y. Li, Y. Li, N. Hu, S. Ma, S. Hu, P. Zhu, W. Wang, H. Zhou, Yap promotes hepatocellular carcinoma metastasis and mobilization via governing cofilin/F-actin/lamellipodium axis by regulation of JNK/Bnip3/SERCA/CaMKII pathways, Redox Biol 14 (2018) 59-71.
[75] L. Wang, L. Han, Z. Tao, Z. Zhu, L. Han, Z. Yang, H. Wang, D. Dai, L. Wu, Z. Yuan, T. Chen, The curcumin derivative WZ35 activates ROS-dependent JNK to suppress hepatocellular carcinoma metastasis, Food Funct 9(5) (2018) 2970-2978.
[76] D.C. Kahraman, E. Bilget Guven, P.S. Aytac, G. Aykut, B. Tozkoparan, R. Cetin Atalay, A new triazolothiadiazine derivative inhibits stemness and induces cell death in HCC by oxidative stress dependent JNK pathway activation, Sci Rep 12(1) (2022) 15139.
[77] M. Das, D.S. Garlick, D.L. Greiner, R.J. Davis, The role of JNK in the development of hepatocellular carcinoma, Genes Dev 25(6) (2011) 634-45.
[78] M. Vidal, L. Salavaggione, L. Ylagan, M. Wilkins, M. Watson, K. Weilbaecher, R. Cagan, A role for the epithelial microenvironment at tumor boundaries: evidence from Drosophila and human squamous cell carcinomas, Am J Pathol 176(6) (2010) 3007-14.

[79] H. Teramoto, P. Crespo, O.A. Coso, T. Igishi, N. Xu, J.S. Gutkind, The small GTP-binding protein rho activates c-Jun N-terminal kinases/stress-activated protein kinases in human kidney 293T cells. Evidence for a Pak-independent signaling pathway, J Biol Chem 271(42) (1996) 25731-4.
[80] D. Kim, D.M.J.O. Helfman, Loss of MLCK leads to disruption of cell–cell adhesion and invasive behavior of breast epithelial cells via increased expression of EGFR and ERK/JNK signaling, 35(34) (2016) 4495-4508.
[81] Y. Xin, K. Li, M. Huang, C. Liang, D. Siemann, L. Wu, Y. Tan, X. Tang, Biophysics in tumor growth and progression: from single mechano-sensitive molecules to mechanomedicine, Oncogene In press (2023).
[82] P. Beri, A. Popravko, B. Yeoman, A. Kumar, K. Chen, E. Hodzic, A. Chiang, A. Banisadr, J.K. Placone, H. Carter, S.I. Fraley, P. Katira, A.J. Engler, Cell Adhesiveness Serves as a Biophysical Marker for Metastatic Potential, Cancer research 80(4) (2020) 901-911.
[83] H. Zou, Z. Yang, Y.S. Chan, S.A. Yeung, M.K. Alam, T. Si, T. Xu, M. Yang, Single cell analysis of mechanical properties and EMT-related gene expression profiles in cancer fingers, iScience 25(3) (2022) 103917.
[84] Y.L. Han, A.F. Pegoraro, H. Li, K. Li, Y. Yuan, G. Xu, Z. Gu, J. Sun, Y. Hao, S.K. Gupta, Y. Li, W. Tang, X. Tang, L. Teng, J.J. Fredberg, M. Guo, Cell swelling, softening and invasion in a three-dimensional breast cancer model, Nature physics 16(1) (2020) 101-108.
[85] M. Singla, A. Kumar, A. Bal, S. Sarkar, S. Bhattacharyya, Epithelial to mesenchymal transition induces stem cell like phenotype in renal cell carcinoma cells, Cancer cell international 18 (2018) 57.
[86] G.F. Le Bras, K.J. Taubenslag, C.D. Andl, The regulation of cell-cell adhesion during epithelial-mesenchymal transition, motility and tumor progression, Cell adhesion & migration 6(4) (2012) 365-73.
[87] H.T. Nia, L.L. Munn, R.K. Jain, Physical traits of cancer, Science (New York, N.Y.) 370(6516) (2020).
[88] T. Koorman, K.A. Jansen, A. Khalil, P.D. Haughton, D. Visser, M.A.K. Rätze, W.E. Haakma, G. Sakalauskaitė, P.J. van Diest, J. de Rooij, P.W.B. Derksen, Spatial collagen stiffening promotes collective breast cancer cell invasion by reinforcing extracellular matrix alignment, Oncogene 41(17) (2022) 2458-2469.
[89] W. Wang, P.V. Taufalele, M. Millet, K. Homsy, K. Smart, E.D. Berestesky, C.T. Schunk, M.M. Rowe, F. Bordeleau, C.A. Reinhart-King, Matrix stiffness regulates tumor cell intravasation through expression and ESRP1-mediated alternative splicing of MENA, Cell reports 42(4) (2023) 112338.
[90] S. Azadi, M. Tafazzoli Shadpour, M.E. Warkiani, Characterizing the effect of

substrate stiffness on the extravasation potential of breast cancer cells using a 3D microfluidic model, Biotechnology and bioengineering 118(2) (2021) 823-835.
[91] L. Shah, A. Latif, K.J. Williams, E. Mancuso, A. Tirella, Invasion and Secondary Site Colonization as a Function of In Vitro Primary Tumor Matrix Stiffness: Breast to Bone Metastasis, Advanced healthcare materials 12(3) (2023) e2201898.
[92] R.G. Wells, The role of matrix stiffness in regulating cell behavior, Hepatology (Baltimore, Md.) 47(4) (2008) 1394-400.
[93] T. Fuhs, F. Wetzel, A.W. Fritsch, X. Li, R. Stange, S. Pawlizak, T.R. Kießling, E. Morawetz, S. Grosser, F.J.N.P. Sauer, Rigid tumours contain soft cancer cells, 18(12) (2022) 1510-1519.

Figure Captions

Figure 1. Mechanical stiffness of HCC cells is inversely correlated with their migratory and invasive ability. (a) The cellular stiffness of HCC cells measured by AFM. The histograms of Young's modulus with Gaussian fittings showed the distribution of cell stiffness for two HCC cell lines: MHCC97-L (n=117 cells) and HepG2 (n=143 cells). **(b)** The levels of F-actin and pMLC in different HCC cells. F-actin and pMLC were measured using immunofluorescence staining (green; left panel) and the mean fluorescence intensity was quantified in the right panel. n=100 and 95 cells for both F-actin and pMLC in MHCC97-L and HepG2. Scale bar: 25 μm. **(c)** The analysis of cell migration by wound healing assay in MHCC97-L and HepG2. The representative images at 0, 24 and 48 h were shown on the top and the wound closure was analyzed on the bottom. n=3 independent experiments. Scale bar: 200μm. **(d, e)** The migration and invasion of HCC cells in Transwell assay. The migrated and invaded cells were stained by crystal violet in the representative images (left) and the numbers of these cells were calculated (right). n=3 independent experiments. Scale bar: 50μm and 100μm in (d) and (e). All the data were presented as Means ± SEMs. Student t-test was adopted for the statistical analysis. * $p<0.05$, ** $p<0.01$, *** $p<0.001$, **** $p<0.0001$.

Figure 2. Reducing actomyosin activity softens HCC cells and promotes migration and invasion. (a, b) The influence of myosin and ROCK inhibition on actomyosin activity and cellular stiffness. Bleb (10 μM) and Y-27632 (10 μM) were used to treat HepG2 cells for 12 h. The levels of F-actin (a), F-actin/G-actin ratio, pMLC, and cellular stiffness (b) were examined by immunofluorescence staining, immunoblotting, and AFM, respectively. (a-left): representative immunofluorescence images of F-actin (green); Scale bar: 50μm; (a-right): the quantification of mean fluorescence intensity. n=100, 100, and 90 cells for Control, Bleb, and Y-27632. (b-i) F-actin/G-actin ratio; (b-ii): immunoblotting of pMLC, n=3 independent experiments; (b-iii): the Young's modulus of HCC cells, where n=197, 179, and 179 cells for Control, Bleb, and Y-27632. **(c)** Wound healing analysis of HepG2 cells after the treatment of Bleb and Y-27632. n=3 independent experiments. Scale bar: 200μm. **(d-f)** The migration and invasion of HepG2 cells after the treatment of Bleb and Y-27632 measured by Transwell assay. n=3 independent experiments. Scale bar: 100μm. **(g)** Cell invasion in 3D collagen gels. n=3 independent experiments. Scale bar: 200μm. **(h)** The stiffness of HepG2 cells after silencing MLCK or mDia1. The cellular stiffness was measured by AFM. n=255, 166, and 177 cells for Control, si-MLCK, and si-mDia1. **(i)** Wound healing analysis of HepG2 cells after silencing MLCK or mDia1. n=3 independent experiments. Scale bar: 200μm. **(j-l)** Transwell migration and invasion analysis of HepG2 cells after silencing

MLCK or mDia1. n=3 independent experiments. Scale bar: 50μm (top) and 100μm (bottom). The ANOVA analysis was utilized for all the statistics and Bonferroni test was adopted for post hoc analysis. * $p<0.05$, ** $p<0.01$, *** $p<0.001$, **** $p<0.0001$.

Figure 3. Activating actomyosin stiffens HCC cells and impairs motility. (a, b) The effects of Jasp and Narci on actomyosin activity. (a-left): representative immunofluorescence images of F-actin (green), scale bar: 50μm; (a-right): the quantification of fluorescence intensity. n=106, 100, and 105 cells for Control, Jasp and Narci. (b-i): F-actin/G-actin ratio after treatment; (b-ii): immunoblotting analysis of pMLC, n=3 independent experiments; (b-iii): the Young's modulus of HCC cells, where n=197, 185, and 175 cells for Control, Jasp and Narci. **(c-e)** Transwell migration and invasion analysis of HepG2 cells after the treatment of Jasp and Narci. n=3 independent experiments. Scale bar: 100μm. **(f)** The invasion of Huh-7 cells in 3D collagen gels. n=3 independent experiments. Scale bar: 200μm. **(g)** The effect of CA-MLCK and CA-ROCK on cellular stiffness. n=173, 158, and 177 cells for CA-Empty, CA-MLCK and CA-ROCK. **(h)** Wound healing analysis of MHCC97-L cells. n=3 independent experiments. Scale bar: 200 μm. **(i-k)** Transwell migration and invasion analysis of HepG2 cells. n=3 independent experiments. Scale bar: 100 μm. The ANOVA analysis was utilized for all the statistics and Bonferroni test was adopted for post hoc analysis. * $p<0.05$, ** $p<0.01$, *** $p<0.001$, **** $p<0.0001$.

Figure 4. Actomyosin regulates the migration and invasion of HCC cells through the effect on cellular stiffness. (a-c) Transwell migration and invasion of HepG2 cells. HepG2 cells were transfected with MLCK siRNA and then overexpressed with CA-MLCK plasmids. Cell motility was measured by Transwell migration (b) and Transwell invasion (c) assay. n=3 independent experiments. Scale bar: 50μm. **(d-i)** The migration and invasion of CA-MLCK and CA-ROCK HepG2 cells after the treatment of Bleb or CytoD. HepG2 cells were first transfected with CA-Empty, CA-MLCK and CA-ROCK plasmids and then treated with 10 μM Bleb (d-f) or 0.5 μM CytoD (g-i). Cell motility was analyzed by Transwell migration and invasion assay. n=3 independent experiments. Scale bar: 100μm. **(j-l)** The influence of F-actin polymerization on the motility of HepG2 cells after the inhibition of MLCK or mDia1. HepG2 cells were first transfected with the siRNAs of MLCK or mDia1, and then treated with 0.1 μM Jasp. Cell migration and invasion were analyzed by Transwell assays. n=3 independent experiments. Scale bar: 100μm. The ANOVA analysis was utilized for all the statistics and Bonferroni test was adopted for post hoc analysis. * $p<0.05$, ** $p<0.01$, *** $p<0.001$, **** $p<0.0001$, n.s.: no significance.

Figure 5. Actomyosin-mediated cellular stiffness regulates motility through JNK signaling. (a-c) The effects of cell softening and stiffening on the activity of JNK signaling. HepG2 cells were first transfected with the siRNAs of MLCK and mDia1 or CA-MLCK and CA-ROCK plasmids. The expressions of MKK4, MKK7 and JNK2 were measured by qPCR (a, b; n=3 independent experiments), and the total and phosphorylated amounts of JNK were detected by western blotting (c; representative of two independent experiments). **(d-f)** The influence of JNK activation on the motility of HCC cells after silencing MLCK and mDia1. HepG2 cells were first transfected with the siRNAs of MLCK and mDia1 and then treated with 50 nM Anisomycin (JNK activator). Cell migration and invasion were measured by Transwell assays. n=3 independent experiments. Scale bar: 50μm. **(g-i)** The influence of JNK inhibition on the motility of HepG2 cells after myosin activation. HepG2 cells were first transfected with CA-MLCK and CA-ROCK plasmids and then treated with 20 nM SP600125 (JNK inhibitor). Cell migration and invasion were measured by Transwell assays. n=3 independent experiments. Scale bar: 100μm. The ANOVA analysis was utilized for all the statistics and Bonferroni test was adopted for post hoc analysis. * $p<0.05$, ** $p<0.01$, *** $p<0.001$, **** $p<0.0001$, n.s.: no significance.

Figure 6. Stiffening HCC CSCs reduces the migration and invasion through elevating JNK phosphorylation. (a) The stiffness of HepG2 cells and the derived CSCs. HepG2 cells were cultured in 90-Pa 3D fibrin gels for 7 days to obtain the derived CSCs. The cellular stiffness was measured by AFM. Left: the histograms of Young's modulus with Gaussian fittings; right: the comparison of cell stiffness between HepG2 cells (non-CSC) and CSCs. n= 163 and 188 cells for non-CSC and CSC. **(b-d)** The migration and invasion of HCC cells and their CSCs measured by Transwell assays. n=3 independent experiments. Scale bar: 100 μm (top) and 50 μm (bottom). **(e)** The levels of F-actin and phosphorylated JNK in HepG2 non-CSC and CSCs. The intensity of phosphorylated JNK was quantified in the right panel. n=100 cells per condition. Scale bar: 20 μm. **(f-h)** The effects of JNK activation on migration and invasion. HepG2 non-CSC and CSCs were treated with 50 nM Anisomycin or DMSO. The migration and invasion of the treated cells were measured by Transwell assays. n=3 independent experiments. **(i)** The stiffness of CSCs after the overexpression of CA-MLCK and CA-ROCK plasmids. n=130, 127, and 131 cells for CA-Empty, CA-MLCK and CA-ROCK. **(j-l)** The influence of myosin activation on CSC motility. CSCs were transfected with CA-Empty, CA-MLCK or CA-ROCK plasmids. The migration and invasion of these cells were analyzed by Transwell assays. n=3 independent experiments. Scale bar: 100 μm. **(m-o)** The effect of myosin activation on the levels of F-actin polymerization and

JNK phosphorylation. The mean fluorescence intensities of phosphorylated JNK and F-actin (m) were quantified in (n) and (o), respectively. n=75, 91, and 96 cells for CA-Empty, CA-MLCK and CA-ROCK in (n) and 100, 100, and 100 cells for CA-Empty, CA-MLCK and CA-ROCK in (o). **(p-r)** The influence of JNK inhibition on the motility of CSCs after myosin activation. CSCs were transfected with CA-Empty, CA-MLCK or CA-ROCK plasmids, and then treated with 20 nM SP600125. Cell migration and invasion were measured by Transwell assays. n=3 independent experiments. Scale bar: 100μm. Student t-test was adopted for the statistical analysis in (a-e) and the ANOVA analysis was utilized for the statistics with Bonferroni test for post hoc analysis in (g-r). * $p<0.05$, ** $p<0.01$, *** $p<0.001$, **** $p<0.0001$, n.s.: no significance.

Fig. 1

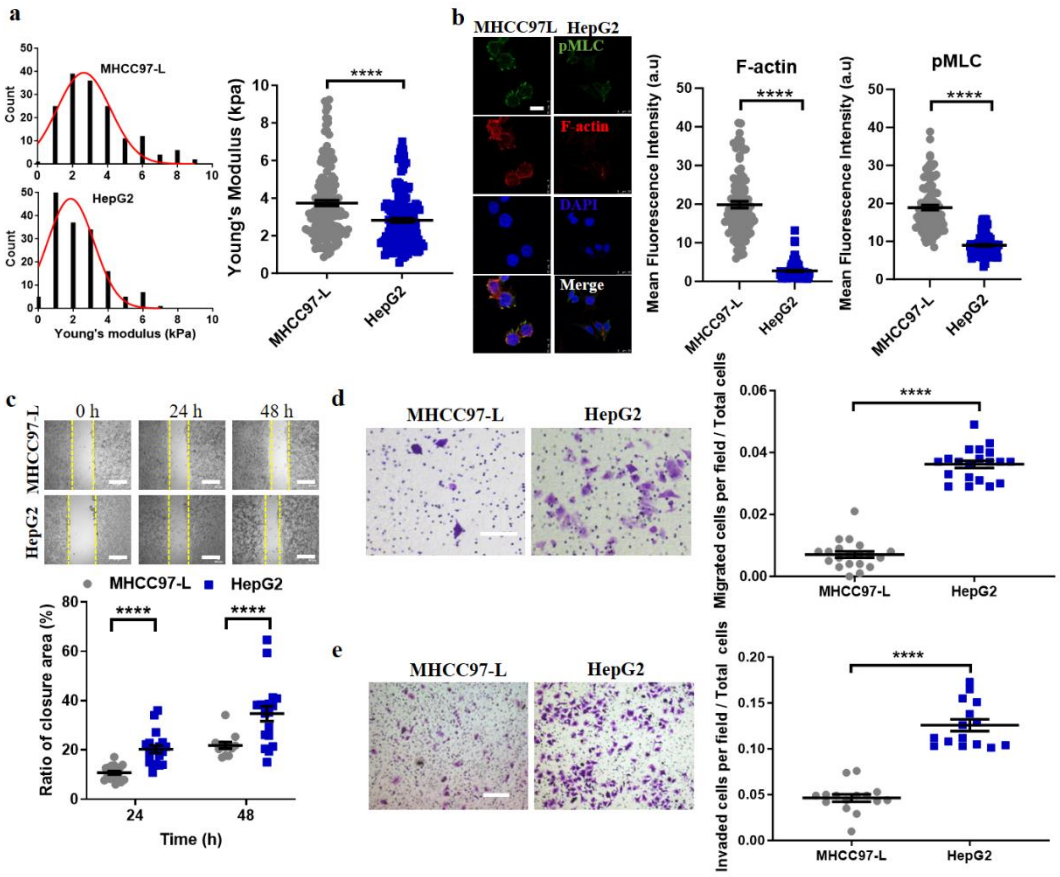
a
MHCC97-L
HepG2
Count
Young's modulus (kPa)
Young's Modulus (kpa)
****
MHCC97-L
HepG2
b
MHCC97L
HepG2
pMLC
F-actin
DAPI
Merge
Mean Fluorescence Intensity (a.u)
F-actin
pMLC
****
c
0 h
24 h
48 h
MHCC97-L
HepG2
Ratio of closure area (%)
Time (h)
d
Migrated cells per field / Total cells
e
Invaded cells per field / Total cells

Fig. 2

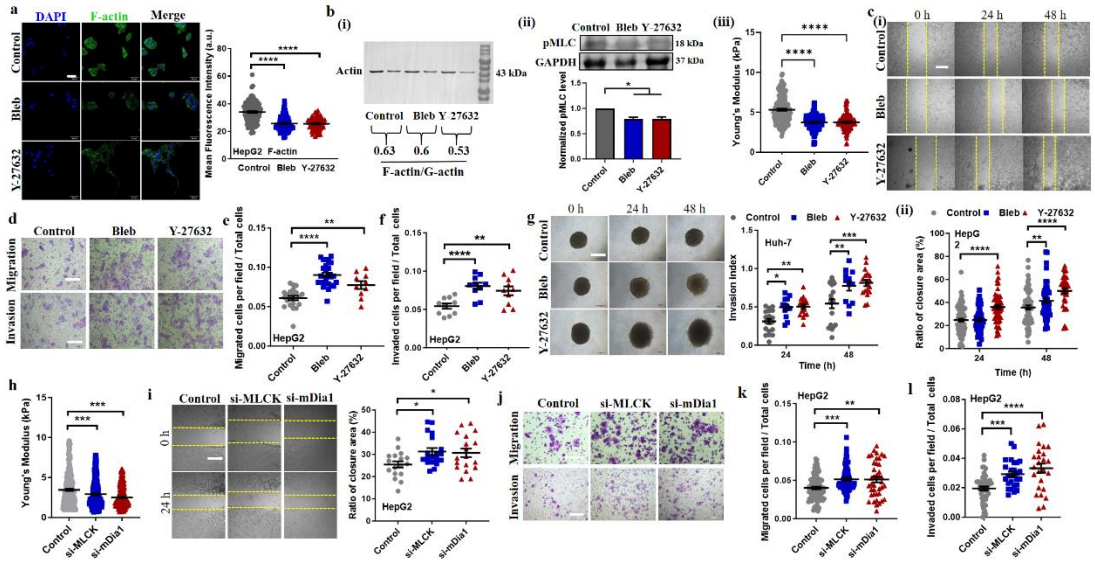
a
DAPI
F-actin
Merge
Control
Bleb
Y-27632
Mean Fluorescence Intensity (a.u.)
HepG2 F-actin
b
(i)
Actin
43 kDa
0.63
0.6
0.53
F-actin/G-actin
(ii)
pMLC
GAPDH
18 kDa
37 kDa
Normalized pMLC level
(iii)
Young's Modulus (kPa)
c
(i)
0 h
24 h
48 h
d
Migration
Invasion
e
Migrated cells per field / Total cells
HepG2
f
Invaded cells per field / Total cells
g
Huh-7
Invasion Index
Time (h)
(ii)
HepG
Ratio of closure area (%)
h
si-MLCK
si-mDia1
i
j
k
l

Fig. 3

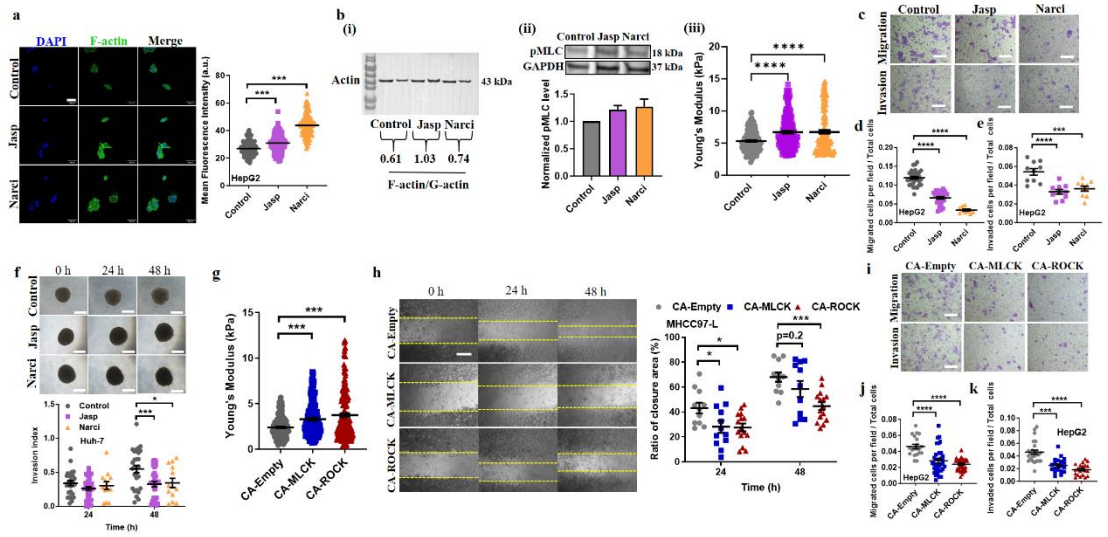
a
DAPI
F-actin
Merge
Control
Jasp
Narci
Mean Fluorescence Intensity (a.u.)
HepG2
b
(i)
Actin
43 kDa
Control Jasp Narci
0.61 1.03 0.74
F-actin/G-actin
(ii)
Control Jasp Narci
pMLC
GAPDH
18 kDa
37 kDa
Normalized pMLC level
(iii)
Young's Modulus (kPa)
c
Control
Jasp
Narci
Invasion
Migration
d
Migrated cells per field / Total cells
e
Invaded cells per field / Total cells
f
0 h
24 h
48 h
Control
Jasp
Narci
Huh-7
Invasion index
Time (h)
g
Young's Modulus (kPa)
CA-Empty
CA-MLCK
CA-ROCK
h
0 h
24 h
48 h
CA-Empty
CA-MLCK
CA-ROCK
MHCC97-L
Ratio of closure area (%)
p=0.2
Time (h)
i
CA-Empty
CA-MLCK
CA-ROCK
Invasion
Migration
j
Migrated cells per field / Total cells
k
Invaded cells per field / Total cells
HepG2

Fig. 4

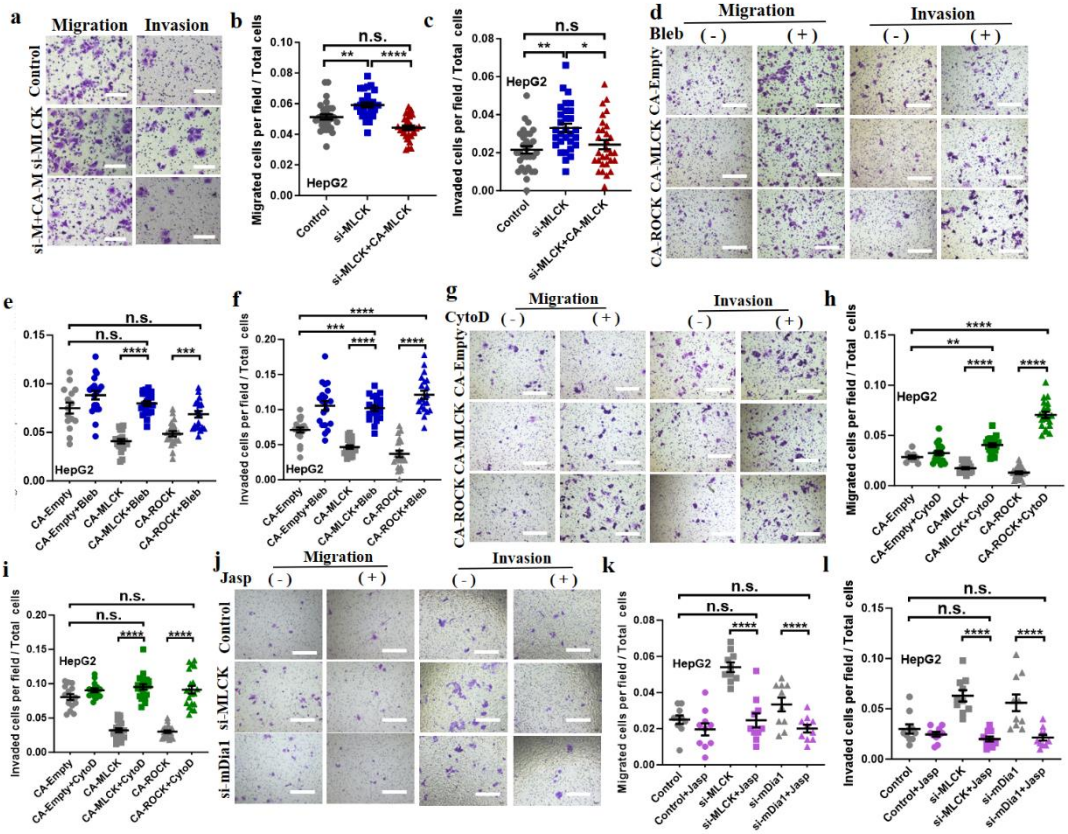
a
Migration
Invasion
Control
si-MLCK
si-M+CA-M
b
Migrated cells per field / Total cells
n.s.
HepG2
Control
si-MLCK
si-MLCK+CA-MLCK
c
Invaded cells per field / Total cells
n.s
HepG2
d
Migration
Invasion
Bleb
CA-Empty
CA-MLCK
CA-ROCK
e
HepG2
CA-Empty
CA-Empty+Bleb
CA-MLCK
CA-MLCK+Bleb
CA-ROCK
CA-ROCK+Bleb
f
Invaded cells per field / Total cells
g
CytoD
h
Migrated cells per field / Total cells
CA-Empty+CytoD
CA-MLCK+CytoD
CA-ROCK+CytoD
i
Invaded cells per field / Total cells
j
Jasp
si-mDia1
k
Migrated cells per field / Total cells
Control+Jasp
si-MLCK+Jasp
si-mDia1+Jasp
l
Invaded cells per field / Total cells

Fig. 5

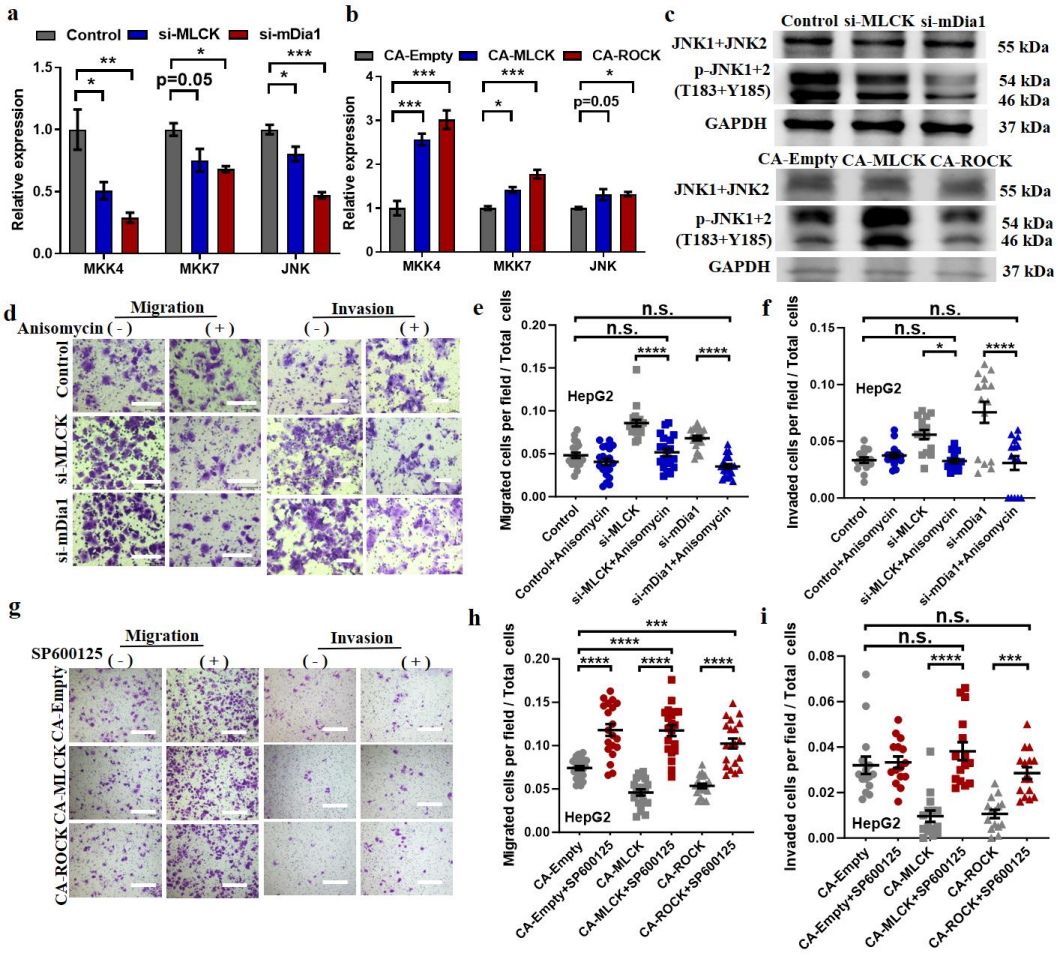
a
Control
si-MLCK
si-mDia1
Relative expression
MKK4
MKK7
JNK
p=0.05
b
CA-Empty
CA-MLCK
CA-ROCK
c
Control si-MLCK si-mDia1
JNK1+JNK2
p-JNK1+2 (T183+Y185)
GAPDH
55 kDa
54 kDa
46 kDa
37 kDa
CA-Empty CA-MLCK CA-ROCK
d
Migration
Invasion
Anisomycin (-) (+)
Control
si-MLCK
si-mDia1
e
Migrated cells per field / Total cells
HepG2
n.s.
Control
Control+Anisomycin
si-MLCK
si-MLCK+Anisomycin
si-mDia1
si-mDia1+Anisomycin
f
Invaded cells per field / Total cells
g
SP600125
CA-Empty
CA-MLCK
CA-ROCK
h
CA-Empty
CA-Empty+SP600125
CA-MLCK
CA-MLCK+SP600125
CA-ROCK
CA-ROCK+SP600125
i

Fig. 6

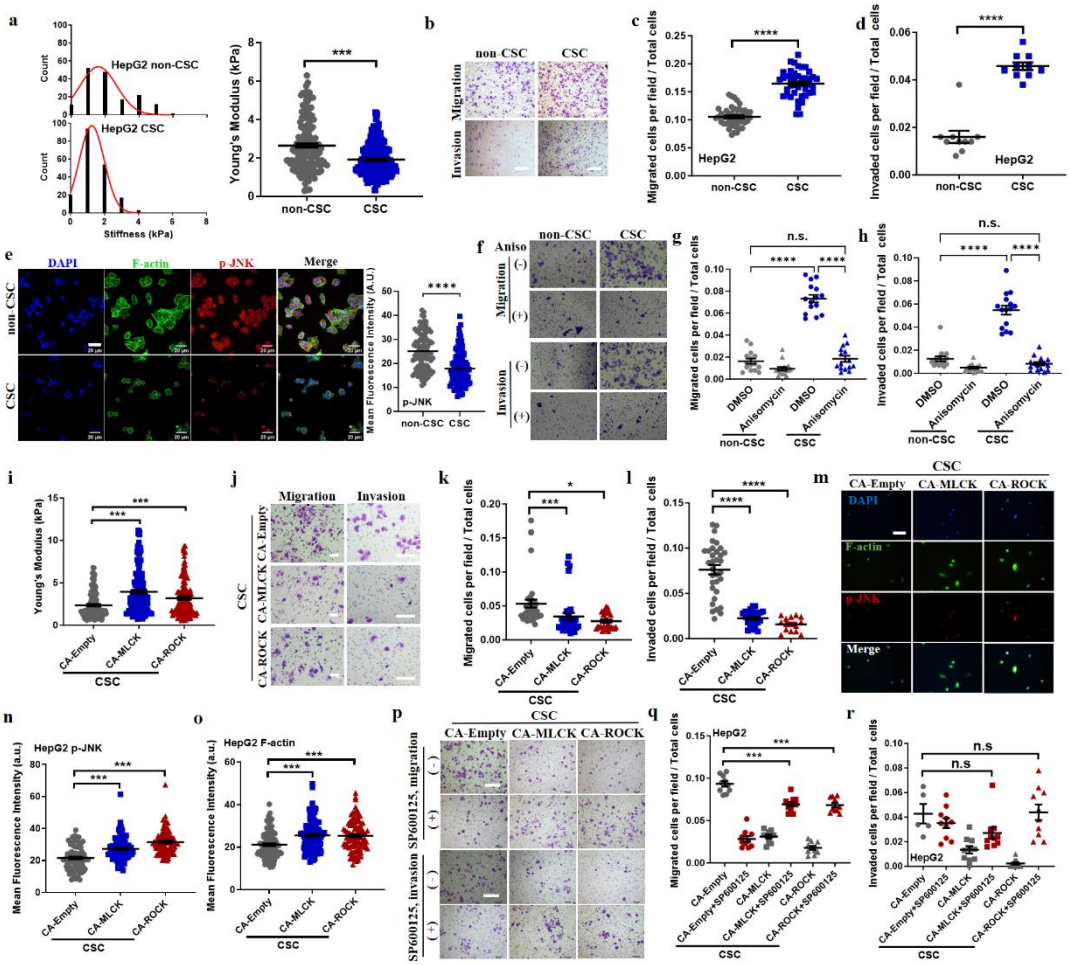
a
HepG2 non-CSC
HepG2 CSC
Count
Stiffness (kPa)
Young's Modulus (kPa)
non-CSC
CSC
b
non-CSC
CSC
Migration
Invasion
c
Migrated cells per field / Total cells
HepG2
d
Invaded cells per field / Total cells
HepG2
e
DAPI
F-actin
p-JNK
Merge
non-CSC
CSC
Mean Fluorescence Intensity (A.U.)
f
Aniso
Migration
Invasion
g
Migrated cells per field / Total cells
n.s.
DMSO
Anisomycin
h
Invaded cells per field / Total cells
i
Young's Modulus (kPa)
CA-Empty
CA-MLCK
CA-ROCK
CSC
j
Migration
Invasion
k
Migrated cells per field / Total cells
l
Invaded cells per field / Total cells
m
CSC
CA-Empty
CA-MLCK
CA-ROCK
DAPI
F-actin
p-JNK
Merge
n
HepG2 p-JNK
Mean Fluorescence Intensity (a.u.)
o
HepG2 F-actin
p
SP600125, migration
SP600125, invasion
q
HepG2
Migrated cells per field / Total cells
CA-Empty+SP600125
CA-MLCK+SP600125
CA-ROCK+SP600125
r
n.s
Invaded cells per field / Total cells